JVST A
Journal of Vacuum Science & Technology A

Retarded solid state dewetting of thin bismuth films with oxide capping layer

Cite as: J. Vac. Sci. Technol. A **39**, 043412 (2021); https://doi.org/10.1116/6.0001048
Submitted: 25 March 2021 • Accepted: 13 May 2021 • Published Online: 01 June 2021

Constantin Wansorra and Wolfgang Donner

JVST A
Journal of Vacuum Science & Technology A

ARTICLE

avs.scitation.org/journal/jva

Retarded solid state dewetting of thin bismuth films with oxide capping layer

Cite as: J. Vac. Sci. Technol. A 39, 043412 (2021); doi: 10.1116/6.0001048
Submitted: 25 March 2021 · Accepted: 13 May 2021 ·
Published Online: 1 June 2021

Constantin Wansorra[a] and Wolfgang Donner

AFFILIATIONS

Materials Science, Structure Research, TU Darmstadt, Alarich-Weiss-Str. 2, 64287 Darmstadt, Germany

[a]**Electronic mail:** constantin.wansorra@tu-darmstadt.de

ABSTRACT

We present a study of the impeding influence of a capping, native oxide layer on the solid state dewetting of thin bismuth films on silicon (111) in vacuum. We study the temperature dependence of the film thickness and strain of the thin films through the analysis of crystal truncation rods of clean and capped bismuth films. This analysis reveals a dewetting temperature difference of 40 °C between capped and uncapped films. The results are supported by scanning electron microscopy and x-ray photoelectron spectroscopy experiments. Furthermore, a model for the retarding effect of the oxide layer and the final shape of the thin film is presented.

I. INTRODUCTION

Solid state dewetting of thin films at elevated temperatures is investigated with increasing experimental and theoretical effort for several reasons. First, the resulting networks,[1] nanowires,[2] and nanoparticles[3–5] show interesting properties and can be created with relative ease and steadily increasing control.[6] Furthermore, knowledge about the prevention of solid state dewetting can be important for applications of thin films at elevated temperatures, because dewetting is a possible destruction mechanism for thin films. A straightforward way to increase the dewetting temperature is to increase the film thickness.[7] In cases where the increase in the film thickness is not possible, the most promising way to prevent dewetting is to inhibit surface diffusion, which is the dominating and rate determining mechanism for solid state dewetting. It has been shown that this can be done either by adsorption of immobile adsorbates[6] or by capping with a graphene layer.[8] In the present study, we show that it is also possible, under certain circumstances, to increase the dewetting temperature by a capping of the thin film with its native oxide.

We present a study about the retarded solid state dewetting of thin bismuth(0001) films with the oxide capping layer on Si(111) substrates and compare the dewetting dynamics to reference samples without the oxide capping layer. The analysis of the dewetting process is done by fitting a model to crystal truncation rods measured *in situ* by x-ray diffraction (XRD). We were hereby able to determine the thickness of a thin film with atomic resolution, which can be connected to the surface coverage of the sample due to volume conservation. Furthermore, scanning electron microscopy (SEM), x-ray photoelectron spectroscopy (XPS), and electron diffraction have been carried out *ex situ* to analyze the final morphology of the thin films and the type of the oxide layer before and after dewetting. For a detailed description of the fitting of the model to the XRD data, the reader is referred to the supplementary material.[9]

II. EXPERIMENT

The samples were prepared in a Riber EVA 32 ultrahigh vacuum (UHV) chamber with a base pressure below 10^{-10} mbar. The silicon substrates were held at 600 °C for 1 h to evaporate surface adsorbates, followed by a flashing process, in which the samples were flash heated to 1250 °C to remove the native oxide of the surface. This process was repeated until the reflection high energy electron diffraction (RHEED) pattern of the Si(111)-7 × 7 reconstruction was clearly visible. The rapid heating was accomplished by electron beam heating and controlled with a thermocouple pressed to the backside of the sample by a spring. During the entire process, the chamber pressure was kept below 2×10^{-9} mbar. After the substrates were allowed to cooldown to room temperature, they were coated with bismuth by molecular beam epitaxy (MBE) at a rate of 0.11 nm min^{-1}. The growth of the thin films was controlled *in situ* by RHEED and followed the growth mechanism reported by Refs. 10–12. After the formation of

an amorphous wetting layer, pseudocubic and hexagonal islands grow until they reach a critical thickness of 2–8 bilayers. At this thickness, the film transforms into a hexagonal phase with a flat surface and a two-domain structure. The two domains appear because of the two rotational possibilities of the second atomic layer of the hexagonal Bi(0001) surface rotated by 30° to each other. This results in a sixfold diffraction pattern, in which every other reflection originates from a different domain.

After thin film preparation, the reference samples were transferred through vacuum to a transportable mini UHV chamber with beryllium window, whereas the other samples were exposed to air for 5 min before they were transferred in vacuum to the aforementioned mini UHV chamber. Both types of samples were analyzed by XRD inside the UHV chamber with a self-built high-load six circle diffractometer with Mo x-ray tube. Measurements of asymmetric crystal truncation rods were carried out at a constant incident angle of 0.5°, at which the highest intensity of the Bi $01\bar{1}2$ reflection was measured, while the in- and out-of-plane angles were rotated to change the scattering vector. Therefore, four truncation rods of the Bi(0001) thin film were captured: the $10\bar{1}1$ and the $10\bar{1}4$ reflection of the first domain and the $01\bar{1}2$ and the $01\bar{1}5$ reflection of the second domain. The samples were dewetted by an annealing procedure, in which they were heated to subsequently increasing temperatures from 175 to 260 °C, while all XRD measurements were carried out at 100 °C, a temperature assumed low enough to stop the dewetting process. The samples were kept for 1 h at each temperature step. All XRD measurements took place in the transportable mini UHV chamber, in which the pressure during the heating was kept below 10^{-7} mbar, while the temperature was controlled by a thermocouple connected to the backside of the sample by a spring.

After the annealing process was finished, the samples and several reference samples were further analyzed *ex situ* by SEM in a JEOL JSM 7600F and x-ray photoelectron spectroscopy (XPS) in a Phi 5000 Versa Probe. Furthermore, RHEED and low energy electron diffraction experiments were carried out with oxidized and not dewetted films to obtain information about the crystallinity of the oxide layer.

The fitting of the XRD data has been carried out with a self-written Python script and a nonlinear fitting algorithm implemented in scipy.[13] The theoretical x-ray diffractograms of the thin films were calculated by adding up all scattered waves in a *lattice sum*[14] within kinematical scattering theory, which is described in detail in the supplementary material.[9]

III. RESULTS

The resulting x-ray diffractograms of the samples after the first annealing step, together with the corresponding fits, are shown in Fig. 1. It can be seen that the finite thickness Laue fringes of the sample with capping oxide layer are attenuated compared to those of the reference sample. However, it is still possible to obtain an atomic layer resolution in the number of bilayers by fitting the XRD profile. At a q_L-value of 1.06 nm^{-1}, an additional peak can be discerned in the diffractogram of the reference sample that can be assigned to the tail of the substrate Si$1\bar{1}1$ reflection. This reflection is not visible in the diffractogram of the sample with the oxide

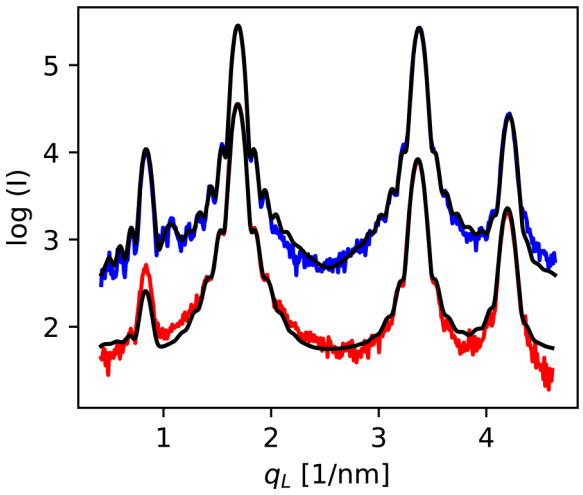

FIG. 1. X-ray diffraction data of the sample with (1, red) and without (2, blue) the oxide capping layer. The corresponding fits are shown in black. Reflections from left to right can be identified by considering the two-domain structure as the $10\bar{1}1$-first domain, $01\bar{1}2$-second domain, $10\bar{1}4$-first domain, and $01\bar{1}5$-second domain reflections of bismuth.

layer because of a rotation of the threefold sample around 60°. Therefore, the first and third reflection of the reference sample originate from the same domain as the second and fourth reflection of the sample with the oxide layer and vice versa. However, this only appears as a factor representing the volume ratio between the two domains and does not affect other results of the fit.

SEM images of the dewetted samples are shown in Fig. 2. While the thin film of the reference sample without the oxide layer still consists of a continuous network, the thin film with the oxide layer appears as completely separated islands, indicating a notable difference in the dewetting mechanism. Higher magnifications reveal that there are many smaller islands with threefold symmetry present in both films.

The measured XPS data of a thin bismuth film with the oxide capping layer before and after dewetting can be seen in Fig. 3. Furthermore, a high resolution spectrum of the bismuth 4f peaks reveals that the oxide layer is still present in the film after dewetting that can be seen at an increasing relative intensity of the bismuth oxide 4f peaks compared to the bismuth 4f peaks. The XPS survey spectrum is also a proof that the thin film only consists of bismuth oxide, apart from small carbon and nitrogen peaks that result from dirt on top of the samples, which was probably caused by the transport to the XPS device.

IV. DISCUSSION

The number of bilayers and the distance between bilayers of the bismuth films resulting from the fits of the temperature dependent XRD data (Fig. 4) show the different dewetting behavior caused by the oxide capping. It can be seen that, in contrast to the thin film without capping, the dewetting of a thin film with the oxide layer is prevented until a critical temperature is reached, at

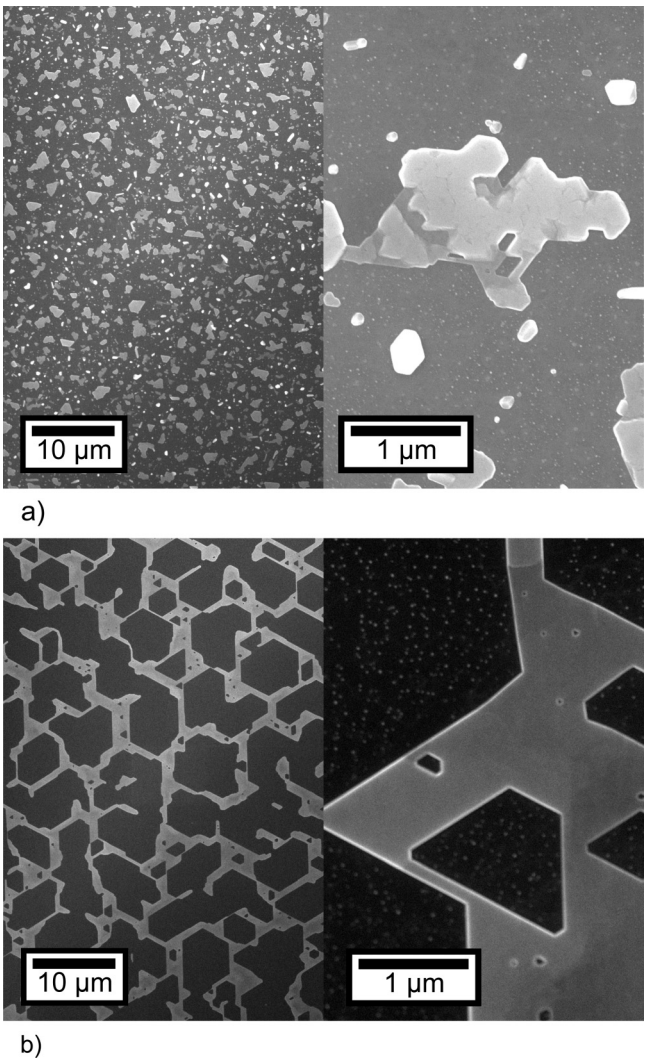

FIG. 2. Scanning electron microscopy images of the dewetted thin films (a) with and (b) without the oxide capping layer during the dewetting. The thin film with the oxide layer dewets into separated small islands, while the thin film without the oxide layer still shows a connected network. Many 120° angles can be seen in both micrographs, indicating the slowest retreating edges fit to a certain direction of the threefold two domain bismuth(0001) thin film.

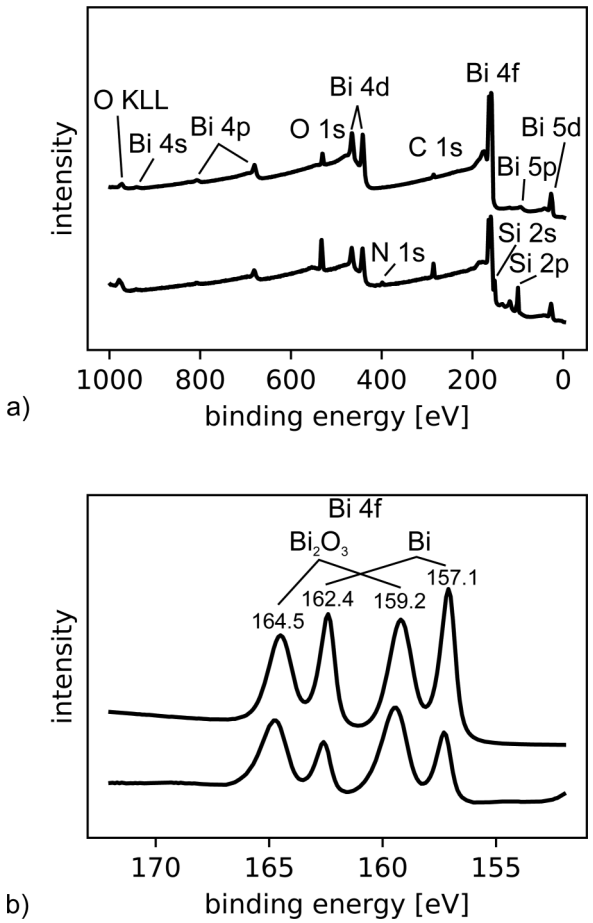

FIG. 3. XPS data of a bismuth thin film on silicon before (top curve) and after (bottom curve) dewetting. (a) The survey spectrum indicates a pure oxide layer on top of the film, which is thinner than the information depth, in contrast to the whole film. (b) High resolution spectrum of the bismuth 4f peaks can be analyzed to calculate the ratio of bismuth oxide and pure bismuth within the information depth. A U2 Tougard-background was used for the fitting.

which the dewetting proceeds rapidly. Furthermore, the number of bilayers of the capped film (and therefore its surface morphology) becomes inhomogeneous at high annealing temperatures. This number can be obtained in different ways: the number of bilayers can either be fitted by using the finite thickness Laue fringes (1, red, hollow circles) or the width of a reflection (1, red, filled circles). The reader is referred to the supplementary material[9] for a detailed discussion of the fitting of the diffraction data. An analysis of the SEM images results in a similar surface coverage of both thin films. While the reference film covers 25% of the sample, the sample with oxide layer is covered 20% by the thin film. Therefore, we conclude that, once the oxide layer barrier is broken, the dewetting is driven by similar kinetics than the sample without the oxide layer. In our opinion, the resulting separated islands are the outcome of a much higher number of nucleation centers, represented by holes in the thin film in solid state dewetting. A higher number of nucleation centers will cause more dewetting edges to be formed simultaneously and therefore increases the possibility of the thin film to dissipate energy by dewetting and resulting in a higher dewetting rate, which can be seen in the slope of curve 1, red, filled circles in Fig. 4(a). Furthermore, the analysis of the strain of the thin films reveals the protecting effect of the oxide layer in more detail. It has been shown in our previous work[15] that thin bismuth films undergo some relaxation process during solid state dewetting, in which the

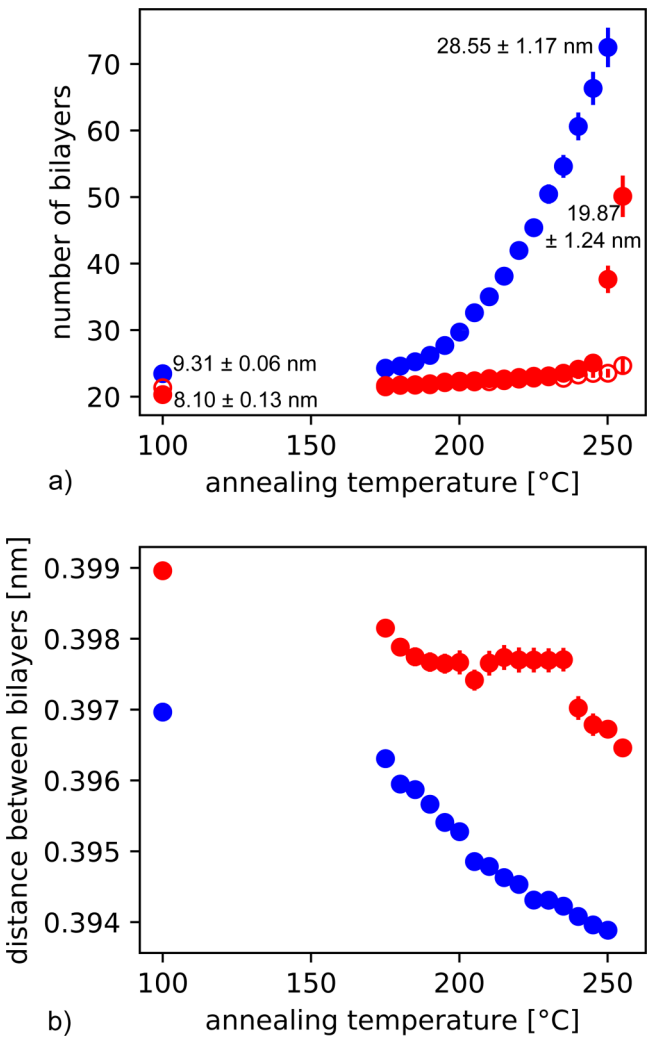

FIG. 4. Results of the fitting of the x-ray diffraction data of a sample with the oxide layer (1, red) and a sample without the oxide layer (2, blue). (a) The number of bilayers plotted by the annealing temperature shows the shift of the dewetting of a sample with the oxide layer to higher temperatures with respect to the dewetting of a sample without the capping layer. (b) The stagnation of the dewetting process of a sample with the oxide capping layer can be seen in a horizontal plateau of the distance between bilayers over the annealing temperature.

misfit strain decreases. In the first approximation, for clean bismuth films this phenomenon appears as a straight line when plotting the distance of the bilayers over the annealing temperature, as it can be seen at curve 2, blue in Fig. 4(b). However, the sample with the oxide layer shows a similar behavior at first [curve 1, red in Fig. 4(b)], until the relaxation process is hindered and the resulting graph becomes horizontal. At a critical temperature of 240 °C, the process starts again, following a straight line, and resulting in a kink in the curve.

Since both bismuth films were prepared with the same growth parameters, the difference of three in the number of bilayers before dewetting (≈1.2 nm) can be assigned to the oxidized layers on top of the film. While *ex situ* LEED and RHEED experiments indicate that the oxide layer is amorphous, analysis of the XPS data shows the chemical shift of Bi_2O_3 at the bismuth 4f peak and that there is no contamination with other elements in the layer. With this information in mind, we designed a model for the dewetting of thin bismuth films with oxide layer capping that is presented in Fig. 5.

The slow increase in the number of bilayers [curve 1, red in Fig. 4(a)] is an indication for more and more holes being generated in the film before the onset of dewetting. An annealing treatment of repeated heating and cooling cycles (like the one in this study) can result in holes in thin films caused by differences in thermal expansion of the thin film and the substrate material. As a result of this, there are weak spots already present in the film at which several diffusion mechanisms are possible that are shown in Fig. 5(a). Since the proceeding dewetting causes edges to move inside (dashed arrows) and because of volume conservation, the thickness of the thin film increases and atoms need to be moved from the bottom of the film to the top. We assume that the influence of bulk diffusion can be neglected since its activation energy is much larger than for surface and interface diffusion. Analyzing the number of bilayers that has been fitted to the last measured XRD pattern, a model for the final film can be created [Fig. 5(b)]. Because the peak shape reveals an average thickness of the film of (50.1 ± 3.1) bilayers, at least some regions of the film must show this thickness (region 1). Furthermore, the analysis of the still present finite thickness Laue fringes reveals areas at which the thickness of the bismuth film is (24.7 ± 1.4) bilayers (region 2). Since the coverage of the surface by the thin film decreases to 1/5th, the thickness of the film needs to be increased by a factor of 5 in average, which includes the thickness of the oxide film. This increase would result in an average oxide film thickness of more than 6 nm, which is expected to be higher than the information depth of the XPS experiment. Because the signal of pure bismuth does not vanish, we assume that those parts of the thin film with high thickness are not covered by the oxide layer anymore. For a quantification of the different areas, the transfer to the XPS spectrometer through air needs to be considered, which results in an oxidization of all open bismuth areas [Fig. 5(c)]. From the XPS measurements, the fraction of bismuth oxide to the XPS intensity increases from 57.09% to 70.84%, from which a fraction of region 2 of 32.04% can be calculated by Eq. (1), with the assumptions that the oxide layer of a dewetted sample is thicker than the information depth of the XPS measurements and that no oxygen is desorbed from the film:

$$\left|\begin{array}{c} A_1 \cdot p_1 + A_2 \cdot p_2 = p_{ges} \\ A_1 + A_2 = 1 \\ p_2 = 1 \end{array}\right| \Rightarrow A_2 = \frac{p_{ges} - p_1}{1 - p_1} = \frac{0.7084 - 0.5709}{1 - 0.5709} = 0.3204. \quad (1)$$

In this equation, the proportion of oxide layer in the signal of the two areas of the model are $p_1 = 0.5709$—the thin film is

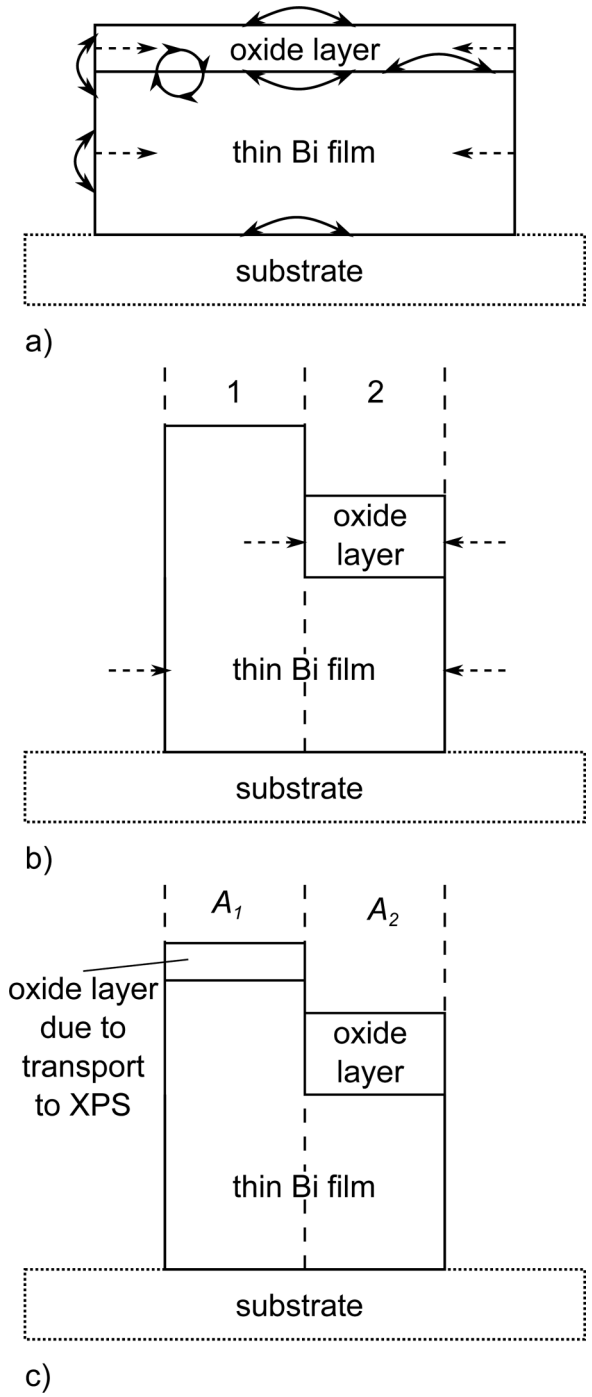

FIG. 5. Model for the solid state dewetting of thin bismuth films with the oxide capping layer. (a) Possible diffusion mechanisms are shown with solid arrows. (b) A possible model for a dewetted film consists of at least two areas that can be discerned in the XRD data. (c) After the transfer to the XPS device through air, the surface of the thin film that is not covered by an oxide layer becomes oxidized.

transferred through air to the XPS system—and $p_2 = 1$, the resulting proportion of oxide signal is p_{ges} and the areas of the model are $A_{1,2}$. This model is supported by SEM images of the dewetted film with the oxide capping layer, which show islands with terraces of different height [Fig. 2(a)].

Using this model as a working hypothesis, we developed a dewetting mechanism in which the thin bismuth oxide film breaks before the entire thin film can change its morphology. This can either happen due to a dewetting of the oxide film or because of a mechanical failure of the oxide film caused by stresses resulting from the heating process. While the oxide film has a high melting temperature, compared with pure bismuth, of 817 °C and therefore should dewet at a high temperature, it is amorphous, very thin, and has preexisting holes in it caused by the relaxation process of the bismuth film, which can all reduce the dewetting temperature of a film. Therefore, we think it is possible that the oxide layer is broken due to solid state dewetting. On the other hand, the annealing process causes mechanical stresses in the thin films due to differences in the thermal expansion of the materials. This may lead to a mechanical failure of the oxide layer, which may also be the reason for the whole process to start. Both mechanisms explain the abrupt increase in the film thickness after reaching the critical temperature of 240 °C and the kink in the curve for the strain relaxation of the thin bismuth film. If the barrier of the oxide layer is broken, the further process can follow the same mechanism as the dewetting of thin bismuth films without the capping layer. However, the oxide layer is still present at some areas and the stagnation of the dewetting caused many holes, which functioned as dewetting seeds. Therefore, the thin bismuth films with and without the oxide layer show a very different appearance after solid state dewetting.

V. CONCLUSION

We have shown that an oxide capping layer is able to increase the dewetting temperature of thin bismuth films on silicon at 40 °C. Based on these data, we designed a model for the dewetting mechanism and the structure of the final film, in which the film can be divided into two regions. According to our model, the velocity determining step is the dewetting of the bismuth oxide layer on top of the bismuth film via surface diffusion, before the remaining bismuth film can finally undergo dewetting. Furthermore, it has been shown that thin bismuth films with the oxide capping layer dewet into separated and small islands at temperatures at which the clean bismuth film still exhibits a connected network of islands.

ACKNOWLEDGMENTS

The execution of scanning electron microscopy by Ulrike Kunz and x-ray photoelectron spectroscopy measurements by Thimo Henning Ferber are gratefully acknowledged.

DATA AVAILABILITY

The data that support the findings of this study are available from the corresponding author upon reasonable request.

REFERENCES

[1]J. Liu, L. Chu, Z. Yao, S. Mao, Z. Zhu, J. Lee, J. Wang, L. A. Belfiore, and J. Tang, Acta Mater. **188**, 599 (2020).
[2]J. Petersen and S. G. Mayr, J. Appl. Phys. **103**, 023520 (2008).
[3]Y.-J. Oh, C. A. Ross, Y. S. Jung, Y. Wang, and C. V. Thompson, Small **5**, 860 (2009).
[4]S. Morawiec, M. J. Mendes, S. Mirabella, F. Simone, F. Priolo, and I. Crupi, Nanotechnology **24**, 265601 (2013).
[5]M. Altomare, N. T. Nguyen, and P. Schmuki, Chem. Sci. **7**, 6865 (2016).
[6]F. Leroy, Ł. Borowik, F. Cheynis, Y. Almadori, S. Curiotto, M. Trautmann, J. Barbé, and P. Müller, Surf. Sci. Rep. **71**, 391 (2016).
[7]C. V. Thompson, Annu. Rev. Mater. Res. **42**, 399 (2012).
[8]P. Cao *et al.*, Adv. Mater. **29**, 1701536 (2017).
[9]See supplementary material at https://www.scitation.org/doi/suppl/10.1116/6.0001048 for a detailed description of the fitting process of the XRD-data.
[10]T. Nagao, T. Doi, T. Sekiguchi, and S. Hasegawa, Jpn. J. Appl. Phys. **39**, 4567 (2000).
[11]M. Kammler and M. H. von Hoegen, Surf. Sci. **576**, 56 (2005).
[12]H. Hirayama, Adv. Phys.: X **6**, 1845975 (2020).
[13]P. Virtanen *et al.*, Nat. Methods **17**, 261 (2020).
[14]I. K. Robinson and D. J. Tweet, Rep. Progr. Phys. **55**, 599 (1992).
[15]C. Wansorra, E. Bruder, and W. Donner, Acta Mater. **200**, 455 (2020).